



Coastal sea-surface wave measurements using software-based GPS reflectometers in Lanyu, Taiwan

Lung-Chih Tsai^{1,2} · Shin-Yi Su¹ · Hwa Chien^{1,3} · Chao-Han Liu⁴ · Harald Schuh^{5,6} · Jens Wickert^{5,6} · Mohamad Mahdi Alizadeh^{5,7}

Received: 24 June 2020 / Accepted: 20 July 2021 / Published online: 3 August 2021
© The Author(s), under exclusive licence to Springer-Verlag GmbH Germany, part of Springer Nature 2021

Abstract

A low-cost transportable software-based global positioning system reflectometry (GPS-R) scheme, which can measure sea-surface wave frequency, period, and speed, is proposed and described. We designed and implemented an appropriate software receiver to acquire and track GPS-R L1-band C/A code signals in near real time. At Lanyu, Taiwan, a research platform has been built with two software-based GPS-R receivers overlooking the seas in the east-northeast and southwest directions. Additionally, we propose applying the maximum entropy method for the spectral analyses of recorded time series of GPS-R signal acquisition data and derive the mean frequencies, periods, and speeds of random sea-surface waves. The derived sea-surface wave frequencies have been compared and validated against buoy measurements and Weather Research and Forecasting (WRF) model data around Lanyu Island. The results show that the buoy wave heights and the modeled WRF wave heights have linear correlation coefficients of 0.64 and 0.47, respectively, with the GPS-R wave frequency measurements. The observed coastal sea area has a maximum horizontal distance of approximately 20 km from station Lanyu (22.037°N, 121.559°E). Thus, the corresponding mapping products of the sea-surface wave period and speed are presented with wave propagation footprints of the first Fresnel zone sizes.

Keywords GNSS reflectometry · Software-based GPS/GNSS receiver · Random sea-surface wave measurement · GPS L1-band C/A code signal acquisition

Introduction

Global positioning system (GPS) or global navigation satellite systems (GNSS) signals have been successfully used worldwide for navigation positioning and timing purposes. However, GPS/GNSS signals can be used to remotely sense geophysical parameters due to the multipath effects of being reflected and/or scattered over the earth's surface. This technique is commonly referred to as GPS reflectometry (GPS-R) or GNSS reflectometry (GNSS-R) and was first introduced for mesoscale altimetry by Martín-Neira (1993). Different approaches of the GPS-R/GNSS-R technique have been proposed for several remote sensing applications, especially to derive ocean altimetry and sea state (Lin et al. 1999; Zavorotny and Voronovich 2000; Rius et al. 2002; Clarizia et al. 2014; Wickert et al. 2016).

In the earlier investigations mentioned above, the basic GPS-R observations include time-delay waveforms or delay-Doppler maps (DDM) as a two-dimensional reflected and scattered power distribution function: one coordinate is

✉ Lung-Chih Tsai
lctsai@csrsr.ncu.edu.tw

¹ GPS Science and Application Research Center, National Central University (NCU), Chung-Li, Taiwan

² Center for Space and Remote Sensing Research, NCU, Chung-Li, Taiwan

³ Graduate Institute of Hydrological and Oceanic Sciences, NCU, Chung-Li, Taiwan

⁴ Academia Sinica, Taipei, Taiwan

⁵ Institute of Geodesy and Geoinformation Science, Technische Universität Berlin, Berlin, Germany

⁶ Helmholtz-Centre Potsdam, German Research Centre for Geosciences GFZ, Potsdam, Germany

⁷ Department of Geodesy and Geomatics Eng, K. N. Toosi University of Technology, Tehran, Iran

the pseudorandom noise (PRN) code offset due to the GPS signal propagation time delay, and the other coordinate is the Doppler shift with respect to the carrier frequency. The obtained DDMs have a typical horseshoe-shaped arc on the contour power distribution observed from an airborne or space receiver. The arc tail structure and asymmetry can be captured due to the relative motion between the GPS transmitter and receiver and the sea-/ocean-surface wave and current velocities. Therefore, GPS-R DDM measurements can be used to retrieve the sea-/ocean-surface wave and current velocities. In this study, we developed and installed a software-based GPS-R observation station at the Lanyu Observatory (22.037°N, 121.559°E) of the Central Weather Bureau (CWB), Taiwan. Compared with an airborne/space GPS-R system, station Lanyu is ground-based and stationary and therefore has much smaller viewing footprint areas on the sea surface and smaller Doppler motions from the GPS satellites. The obtained DDMs do not have distinct horseshoe-shaped arcs used to derive sea state parameters and are not reported here.

We present software-based GPS-R signal acquisition and data processing progress, which are developed and proposed to measure and interpret sea-surface wave parameters. Compared with usual commercial GPS receivers, software-based GPS receivers offer added flexibility and versatility by implementing most functions in software (Tsui 2000; Borre et al. 2007). Another advantage of a software-based GPS receiver is a maximum sampling rate of 1000 Hz due to the L1-band Coarse Acquisition (C/A) code duration at 1 ms and is much higher than that of a typical commercial GPS receiver. For these experiments, a research platform in Taiwan is available and includes two GPS-R receivers in Lanyu, Taiwan. The two receiving systems in Lanyu are positioned at the same altitude of 342 m but view the east-northeast (ENE) and southwest (SW) directions at distances of approximately 1 km and 1.5 km inland, respectively. Thus, we call the two GPS-R observation systems the Lanyu-ENE and Lanyu-SW systems. Figure 1 displays the location of station Lanyu, the validation location of the moored buoy, the validation location of Weather Research and Forecasting (WRF) model data, and the digital terrain map of Lanyu Island. Notably, some views from station Lanyu are obscured by nearby hills. The horizontal viewing angles (azimuth) from both the Lanyu-ENE and Lanyu-SW systems over the sea surface are limited to approximately 90° shown by the yellow areas in Fig. 1. The observed coastal sea area ranges from the nearby seashore to the specular point positions with a minimum depression angle of 1°, i.e., a zenith angle of 91°, as seen from the receiving station. Thus, the observed coastal sea area has a maximum horizontal distance of approximately 20 km ($\approx 0.342 / \tan(1^\circ)$ km) from station Lanyu. The left and right panels of Fig. 2 show the GPS-R receiving antenna installations and the views to the sea from

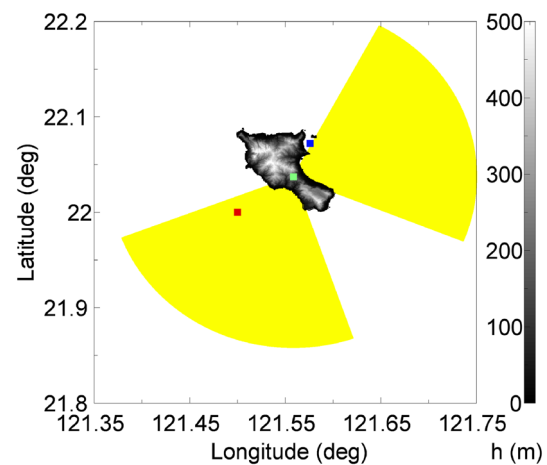


Fig. 1 Horizontal viewing angles and ranges from both the Lanyu-ENE and Lanyu-SW systems over the sea surface are shown separately as yellow areas. We also present the locations of station Lanyu (green square), validation buoy (blue square), and validation WRF model data (red square), and the digital terrain map of Lanyu Island shown in black and white gradients



Fig. 2 GPS-R receiving antenna installations and views to the sea from the Lanyu-ENE (right panel) and Lanyu-SW (left panel) systems

the Lanyu-ENE and Lanyu-SW systems, respectively. Each coastal GPS-R system antenna looks out over the sea at an incident angle 10° lower than grazing and an azimuth angle of approximately 70° (205°) for the Lanyu-ENE (Lanyu-SW) system.

We present a new technique for deriving sea-surface wave frequency and other wave parameters from GPS-R measurements. In the following section, we introduce a software-based GPS-R receiver architecture for sea-surface wave observations and describe the L1-band Coarse Acquisition (C/A) code signal acquisition algorithm using the Fourier transformation correlation theorem. In the subsequent section, we present time-series GPS-R signal acquisition data with random features and propose a maximum entropy

method (MEM) spectral analysis to derive the mean frequency of random waves from sea-surface wave observations. The next section presents the analytical methodology of obtaining GPS-R measurements on sea-surface wave frequency, period, and speed. Subsequently, the derived sea-surface wave frequencies were compared and validated against the in situ buoy measurements and the WRF model data around Lanyu Island. To conclude, we summarize the main conclusions of this paper and point out several problems to be addressed in future studies.

GPS signal acquisition of a software-based GPS-R receiver

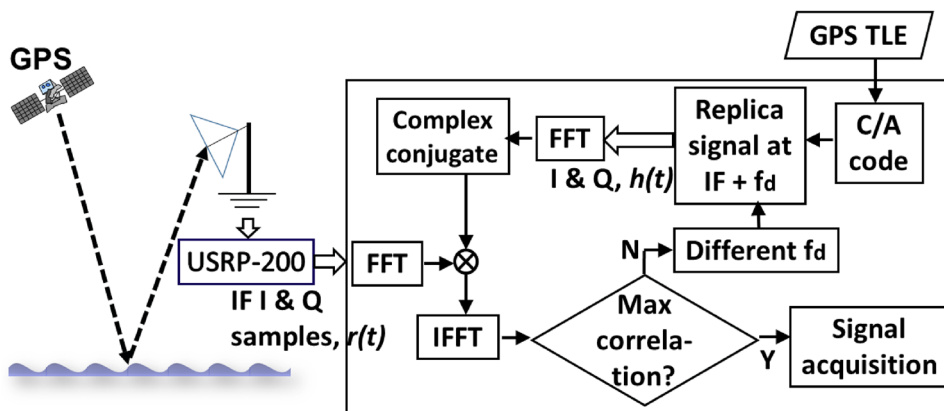
The L1-band Coarse Acquisition (C/A) code signals broadcast by the constellation of GPS satellites have a known structure (Tsui 2000), consisting of a carrier modulated by a pseudorandom noise (PRN) code unique to each of the GPS satellites. A typical software-based GPS-R receiver architecture used to track the L1-band C/A code signals is illustrated in Fig. 3. The GPS signal is transmitted as a right-hand circularly polarized radio wave that becomes left-hand or right-hand elliptically polarized waves after reflection and/or scattering over the sea surface. The reflected and scattered L1-band GPS signal can be received by an applicable antenna and then downconverted, filtered, and digitally sampled by a Universal Software Radio Peripheral B200 (USRP-B200) (<http://ettus.com/all-products/ub200-kit/>) device developed by Ettus Research, a National Instruments Company.

In this study, a dual right-hand and left-hand circular polarization (RHCP/LHCP) L1/L2 GPS antenna (P/N:42G1215RL-AA-5SSF-1) produced by Antcom Corporation (<http://www.antcom.com/>) was installed, but only the LHCP connectivity and its outputs were used on each GPS-R system. We assume that direct signals from a targeted GPS satellite are nearly RHCP waves because its viewing angle, as seen from the receiving antenna, is small, and

their LHCP component signals can be ignored. The signals transmitted to the USRP-B200 module of each GPS-R system are the LHCP components of the left-hand or right-hand elliptically polarized waves reflected and scattered from the targeted ocean. Notably, the viewing depression angle is limited from approximately 15° (10°) to 1° for the Lanyu-ENE (Lanyu-SW) system, as shown in Fig. 1. An earlier investigation (Trizna 1997) derived a virtual Brewster angle with an approximately 5° depression angle for sea echoes at a radio frequency of 1.5 GHz. Thus, the wave polarization of the GPS signal echo is left-hand elliptical at a depression angle larger than 5° and is right-hand elliptical at a depression angle smaller than 5°. The associated LHCP component signal is generally weaker when the viewing depression angle, as seen from station Lanyu, is smaller. Other multipath effects, including reflection from near hills, soil surfaces, and human-made buildings, are possible. However, the corresponding signals are assumed to be nearly constant and weaker than those reflected/scattered from the targeted sea surface. They can be filtered out after signal acquisition and spectral analyses, which are discussed in the following section.

As shown in the block diagram structure of Fig. 3, the sampled digital and complex, i.e., I-Q, signals sent to the PC host physically include different baseband PRN C/A codes from all visible GPS-R satellites. The visible GPS-R satellites are defined as the GPS satellites that have specular reflections located in the targeted sea-surface regions, as shown in the yellow areas in Fig. 1 for station Lanyu. A software-based GPS-R receiver must first determine whether it has reflectometry visibility of certain satellites using known GPS satellite TLE data. The basic GPS C/A code signal acquisition functions in the software algorithms are implemented using a circular correlation in the frequency domain (Tsui 2000). This approach takes advantage of the Fourier transformation correlation theorem, which states that the frequency transform of the correlation function in the time domain is the product of the signals transforming in the frequency domain, as described in the following equation:

Fig. 3 Architecture of a software-based GPS-R receiver for sea-surface wave observations



$$\text{Corr}(r(t), h(t)) \Leftrightarrow R(f) H^*(f) \quad (1)$$

where we use the " \Leftrightarrow " symbol to indicate Fourier transform pairs. As shown in Fig. 3, the I and Q components are combined as complex inputs to a fast Fourier transform (FFT) block. The result of this FFT transform is multiplied by the conjugate of the local PRN C/A code's FFT transform of every visible GPS-R satellite at different satellite Doppler and receiver frequency offsets. Finally, the product is applied to an inverse FFT transform whose maximum magnitude, i.e., the maximum circular correlation value, feeds back to the decision logic. Such signal acquisition could determine the C/A code signal amplitudes, its starting point (or chip delay) compared with the local replica of PRN C/A code, and the associated satellite Doppler and receiver frequency offset of each visible GPS-R satellite. Subsequently, the estimated time delay and associated satellite Doppler and receiver frequency offset are used to track the reflected and/or scattered signals from a targeted GPS satellite. This study only considers the signal acquisition peak tracking measurement hereafter. The acquired and tracked circular correlation values were recorded as time-series data from one GPS-R observation for further data processing.

Spectral analysis of time series of signal acquisition data from GPS-R observations

The instantaneous sea-surface configuration is complex, with wave humps and hollows. Due to the movements of the targeted sea-surface waves and GPS satellites, the GPS-R signal reflection varies with time. Using the circular correlation analysis of the GPS-R signal acquisition, as described in the last section, a time-series record of the maximum correlation value consequently exhibits a random form with many local maxima and minima superposed on irregular undulations from sea-surface waves. Figure 4 shows two colored 67.5-s temporal profiles representing the L1-band C/A code signal acquisition results from visible GPS-R satellite numbers 1 and 11 simultaneously and obtained by the Lanyu-ENE system. It is difficult to define individual waves from such time-series records without some criterion to distinguish a single wave from local humps and hollows. Earlier investigations (Longuet-Higgins 1957; Goda 1990) concluded that randomness is an important feature of sea and ocean waves. The present understanding of random ocean waves is that they are composed of a number of monochromatic waves with various frequencies. We propose derivation of the statistical properties of sea-surface wave parameters using a spectral analysis of the GPS-R signal acquisition results.

We propose using the MEM (Press et al. 1992), also known as the linear predictive and autoregressive methods,

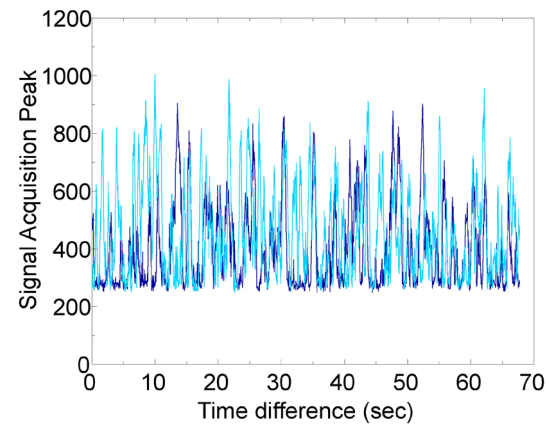


Fig. 4 Example time-series record of L1-band C/A code signal acquisition (in SNR) obtained from the Lanyu-ENE GPS-R system. The dark blue and cyan colored temporal profiles represent the maximum signal acquisition results from visible GPS-R satellite numbers 1 and 11, respectively

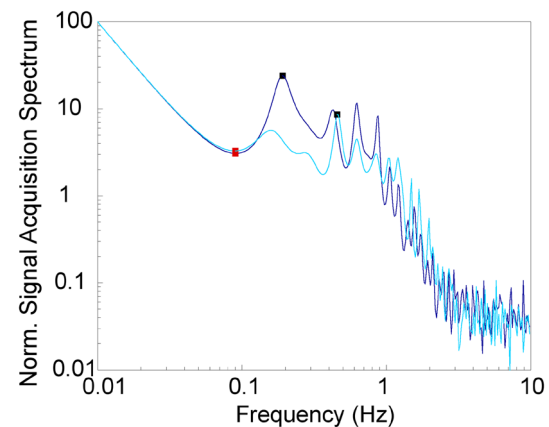


Fig. 5 Log–log plot of the normalized MEM power spectra of the two time series of GPS-R signal acquisition data shown in Fig. 4. The black-colored (red-colored) squares represent the frequencies at the band-limited power spectrum peak (the first local minimum of power spectra) induced by random sea-surface waves

to estimate the power spectra of the experimental time series of the GPS-R signal acquisition data. Figure 5 shows the resulting normalized MEM power spectra of the two time series of GPS-R signal acquisition data used for Fig. 4. We executed GPS L1-band C/A code signal acquisition by circular correlation calculation for every 2 ms of data, i.e., a data recording rate of 500 Hz. Figure 5 focuses on the low-frequency (≤ 10 Hz) part and does not show the 10–250 Hz spectra, which are similar to the spectrum near 10 Hz and exhibit white noise. Notably, both MEM power spectra display a strong dc component and a significant part in the frequency range from approximately 0.1 Hz (the frequency with the first local minimum) to 2 Hz. The later significant

power spectra are believed to be induced by random sea-surface waves in the GPS-R signal observations and cannot be obtained from direct GPS signal observations. As shown, the searched peak wave frequencies (in the black-colored squares) are not stable results for sea-surface wave measurements. Moreover, the order of the MEM is important for spectral analysis resolution and accuracy. In this study, we use an MEM order number of 130, which is approximately one order less than the data number in the time series. The MEM spectrum estimation has a resulting function of continuously varying frequency and essentially increases the spectral resolution. It could be easier and more accurate to specify the spectra induced by random sea-surface waves in GPS-R observations. Therefore, the stochastic approach discussed here is essential to derive the mean wave frequency and wave period through random wave spectral analysis on the estimated MEM power spectra of the GPS-R sea-surface wave observations. According to Rice’s theory (Rice 1944), the mean frequency and period of band-limited waves are given as follows.

$$\bar{f} = \left(\frac{m_2}{m_0} \right)^{0.5}, \bar{T} = \frac{1}{\bar{f}}, \text{ and} \tag{2}$$

$$m_n = \int_{f_1}^{f_2} f^n S(f) df$$

where m_0 and m_2 are the zeroth and second spectral moments, respectively. For the GPS-R sea-surface wave observations shown in Fig. 5, the calculated mean frequencies are 0.62 Hz and 0.82 Hz for GPS satellite numbers 1 and 11, respectively. Notably, the GPS L1-band radio wavelength is much shorter than the horizontal sea-surface wave scale, and the GPS radio signals would be scattered not only at sea-surface wave humps but also hollows. Therefore, when the GPS radio signal interacts with a single sea-surface wave train, the obtained sea-surface wave frequency should be half that of the recorded time series of the signal acquisition data.

Analytical methodology for sea-surface wave frequency, wavelength, and speed determinations

In this study, the GPS-R experiment at Lanyu, Taiwan, collected data over fourteen days from December 12 to 18 and December 20 to 26 in 2019, and both the Lanyu-ENE and Lanyu-SW systems simultaneously executed one 67.5-s duration observation every two minutes. For each reflectometry observation, the reflection will take place at a specular point (SP) position linking the tracked GPS satellite, whose position can be derived by the known GPS satellite TLE data, to the receiving station and over the sea surface.

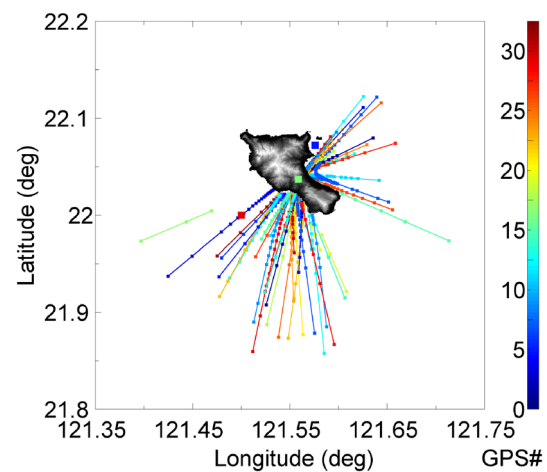
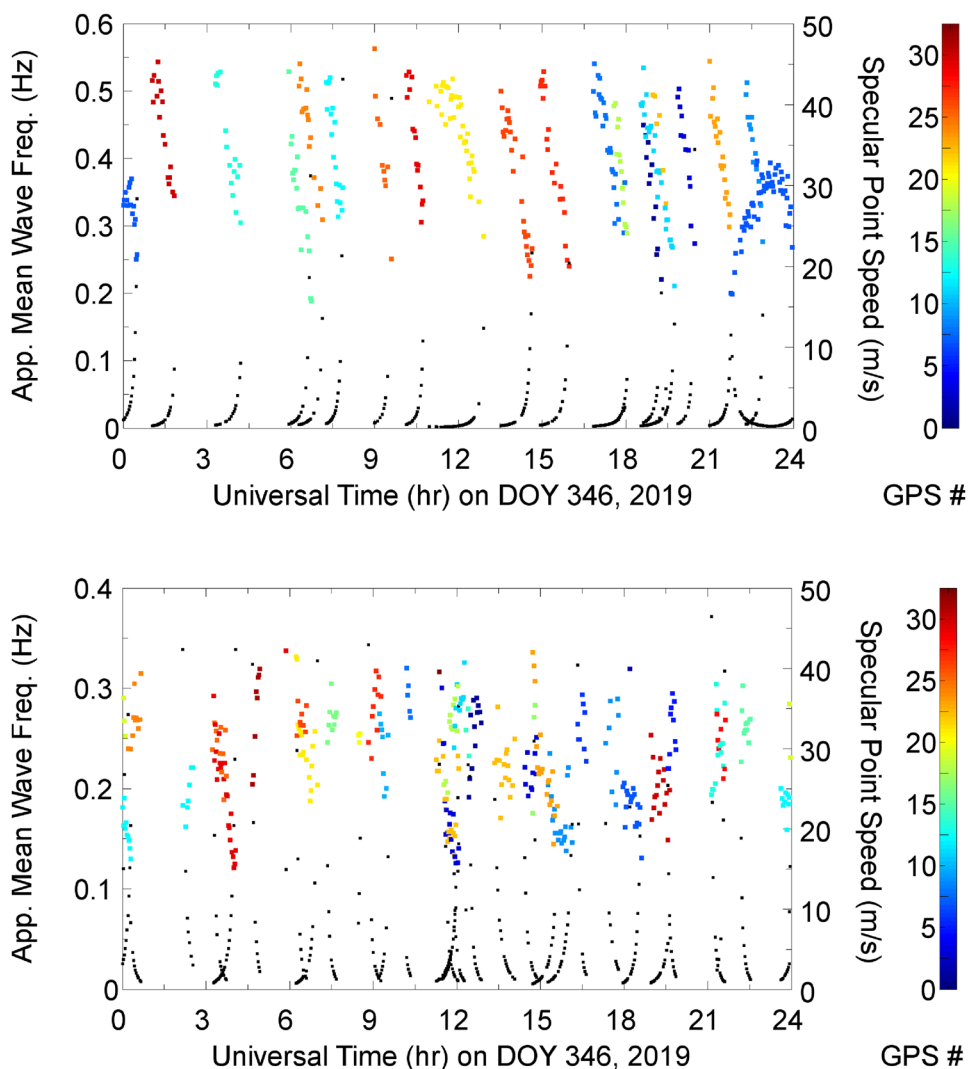


Fig. 6 Tracks of GPS-R SP positions obtained from both the Lanyu-ENE and Lanyu-SW systems on December 12, 2019. The coded colors represent the different GPS-R observations from GPS satellite numbers 1 to 32 as shown as color bar labeled by “GPS #”. As in Fig. 1, the location of station Lanyu, the validation locations of buoy and WRF model data, and the digital terrain map of Lanyu Island are also shown

Figure 6 shows the example SP tracks of the GPS-R observations obtained from both GPS-R systems on December 12, 2019. In the experiment, daily SP track maps are similar to Fig. 6 but change slightly day to day. The longest SP distance seen from the receiving station depends on the minimum depression angle and is also proportional to the station altitude. In this study, we limit the minimum depression angle as seen from the GPS-R station to 1°, i.e. a longest SP distance of approximately 20 km, in which the obtained signal acquisition data have enough significant power spectra induced by random sea-surface waves to derive a reliable mean wave frequency.

Based on the MEM and spectral moment analyses described in the last section, the top and bottom panels of Fig. 7 show the apparent mean wave frequencies f_{app} s versus universal time obtained from the Lanyu-ENE and Lanyu-SW systems, respectively, on December 12, 2019. The figures also show the estimated GPS-R SP speeds, which are estimated by SP position simulation using GPS satellite TLE data and are simply determined by the SP movement distance in one second. As expected, the smaller the observed depression angle is, the longer the SP distance between two continuous GPS-R observations, as shown in Fig. 6, and the higher the SP speed is. Notably, each of the Lanyu-ENE and Lanyu-SW systems can provide more or less than one GPS-R observation. Such an observed satellite number pattern in one day is dependent on the GPS satellite distribution, especially the receiving station site, altitude, and the range and direction of the viewing angles.

Fig. 7 Apparent mean wave frequencies (shown as colored dots and referring to the left y-axis) versus universal time obtained separately from the Lanyu-ENE (top panel) and Lanyu-SW (bottom panel) systems on December 12, i.e., day of year (DOY) 346, 2019. The color coding of the dotted lines represents the different GPS-R observations from GPS satellite numbers 1 to 32. Both figures also show the estimated GPS-R SP speeds (referring to the right y-axis) in black



As shown in Fig. 7, the derived apparent mean wave frequencies f_{app} s are usually distributed but spread along a curve. To produce more reliable f_{app} values, we apply a second-order polynomial as a function of universal time to fit the spread f_{app} values with least-square errors and obtain fitted and interpolated f_{app} values and traces, which are shown with the dotted lines in Fig. 8. Due to the movement of the tracked GPS satellite, the GPS-R SP position varies with time. The obtained reflectometry observations must include the impact of moving SP positions and be mapped in this study from a moving coordinate system to a fixed coordinate system during a GPS-R observation duration of 67.5 s. In principle, we could regulate the apparent mean wave frequency f_{app} from a moving SP platform into a fixed platform and express f_{app} in relation to the final estimated sea-surface wave frequency f_w as follows.

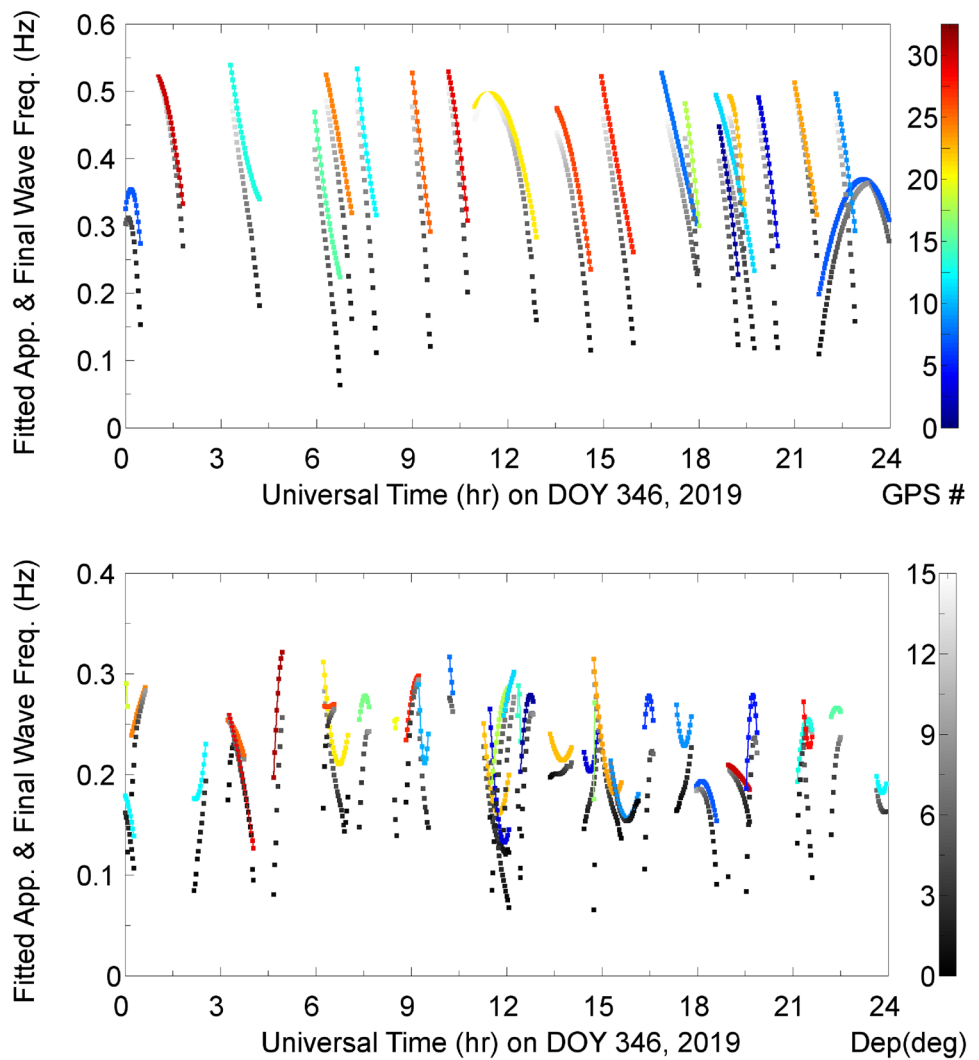
$$f_{app} = \frac{(\bar{V}_w - \bar{V}_{SP}) \cdot \hat{n}_w}{\lambda_w} = f_w - \frac{V_{SPw}}{\lambda_w} \tag{3}$$

where \bar{V}_w , λ_w , and \hat{n}_w are the sea-surface wave velocity, wavelength, and wave normal vector, respectively, and \bar{V}_{SP} and V_{SPw} are the SP velocity and its component in the sea-surface wave direction, respectively. This study assumes that the sea-surface wave direction is consistent with the wind direction, which can be obtained from the Lanyu Observatory, CWB, Taiwan. Moreover, from the hydrodynamical laws (Mei 1990), the following dispersion relationship exists between the sea-surface wave frequency f_w and wavenumber k_w :

$$(2\pi f_w)^2 = g k_w \tanh(k_w h_o) \tag{4}$$

where g is the gravitational acceleration and h_o represents the ocean depth. For the targeted sea area around Lanyu

Fig. 8 Fitted apparent mean wave frequencies (shown as dotted color lines) and final estimated wave frequencies (shown as dots in black and white gradients) versus universal time obtained separately from the Lanyu-ENE (top panel) and Lanyu-SW (bottom panel) systems on December 12, i.e., DOY 346, 2019. The color coding of the dotted lines represents the different GPS-R observations from GPS satellite numbers 1 to 32. The dots coded in black and white gradients represent the depression angles in degrees, as seen from the systems



Island, the ocean bottom is more than one wavelength deep only one hundred meters from the seashore. For such short waves or a deep ocean, i.e., $k_w h_o \gg 1$, the characteristic wavelength can be denoted as follows:

$$\lambda_w \approx \frac{g}{2\pi f_w^2} \tag{5}$$

Then, it is possible to estimate the sea-surface wave frequency f_w by solving the following second-order polynomial equation:

$$f_{app} \approx f_w - \frac{2\pi V_{SPw}}{g} f_w^2 \tag{6}$$

Therefore, we can derive the sea-surface wave period, wavelength, and wave speed. As displayed in Fig. 8 and referring to the fitted apparent wave frequencies, the estimated final wave frequencies as a function of universal

time are also shown and coded by the depression angle in the black and white gradients. Notably, there are usually lower estimated wave frequencies where the depression angles seen from station Lanyu are smaller, i.e., long distances from the station to the GPS-R SP positions. The results are expected because there are usually deeper ocean depths and thus lower sea-surface wave frequencies at greater offshore distances.

Results and validation

Based on the Lanyu-ENE and Lanyu-SW GPS-R observations and sea-surface wave frequency and wavelength measurements, Fig. 9 (Fig. 10) shows the derived sea-surface wave period (speed) maps for December 12 and 18, 2019. The other derived sea-surface wave period and speed maps from December 13–17 during the experiment are transition stages and are not shown in this paper. Notably, the SPs

Fig. 9 Based on the Lanyu-ENE and Lanyu-SW GPS-R measurements, the sea-surface wave period maps obtained on December 12 and 18, 2019, are shown in the left and right panels, respectively. The color coding represents the wave periods from 0 to 20 s. As in Fig. 1, the location of station Lanyu, the validation locations of the buoy and WRF model data, and the digital terrain map of Lanyu Island are also shown

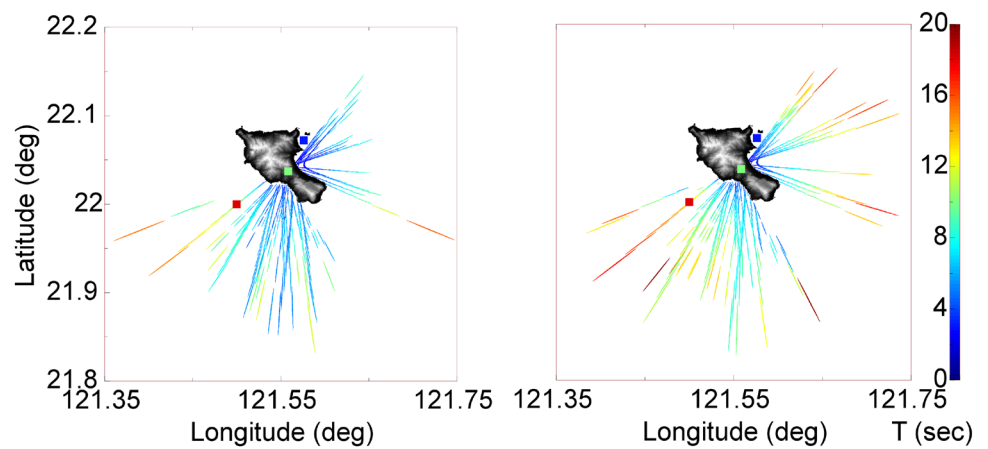
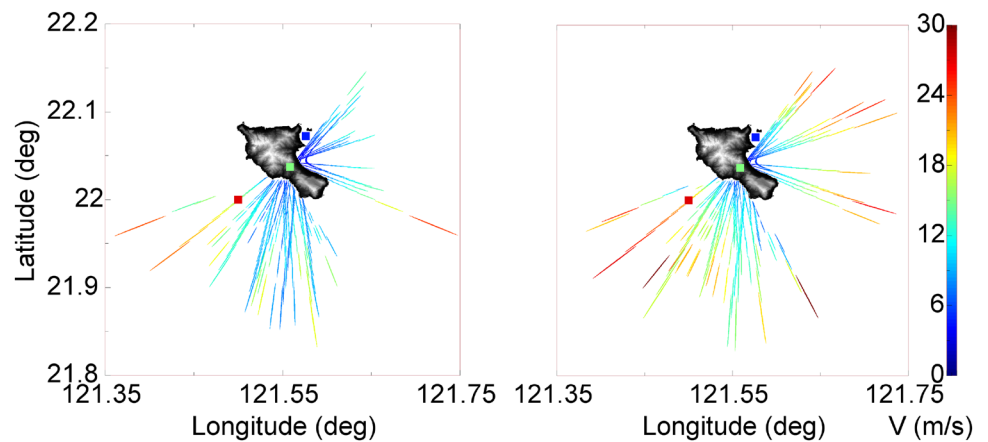


Fig. 10 Based on the Lanyu-ENE and Lanyu-SW GPS-R measurements, the sea-surface wave speed maps obtained on December 12 and 18, 2019, are shown in the left and right panels, respectively. The color coding represents the wave speeds from 0 to 30 m/s



shown in Fig. 6 are the GPS-R reflection points considering radio ray tracing, but this is not the same as the sensing footprint of wave propagation. As shown in Figs. 9 and 10, the footprint of wave propagation and reflection over a flat sea surface for each GPS-R observation is typically estimated by means of Fresnel zone ellipses (Hristov 2000). Usually, the so-called significant propagation region is defined in practice as the first Fresnel zone (FFZ). The FFZ ellipse has an origin point with a radial distance D from the receiving antenna, a major semiaxis a , and a minor semiaxis b onto a sea-surface plane, which are determined as follows:

$$\begin{aligned}
 D &\cong h \times \cot(\theta) \left(1 + \frac{\lambda}{2h \times \sin(\theta)} \right) \\
 a &\cong \frac{1}{\sin(\theta)} \sqrt{\frac{\lambda h}{\sin(\theta)} \left(1 + \frac{\lambda}{4h \times \sin(\theta)} \right)} \\
 b &\cong a \times \sin(\theta)
 \end{aligned}
 \tag{7}$$

where h is the receiving antenna altitude, θ is the depression angle, and λ is the radio wavelength. As shown in Figs. 9 and 10, the FFZ ellipse footprints have major semiaxes that are much larger than the minor semiaxes and have a semiaxis

ratio to be the cosecant of the depression angle, which is from 3.86 to 57.30 in this study. The FFZ ellipse size is larger where the depression angle, as seen from station Lanyu, is smaller. For the sea-surface positions within more than one nearby GPS-R observing footprint, the resulting wave period or speed is the average of those nearby GPS-R measurements. The weights are inverse to ellipse size. Furthermore, the time resolution of such wave period and speed maps is one day. We could improve the time resolution by shortening the mapping duration and decreasing the mapping area. Otherwise, we could build and include more GPS-R receiving stations in future experiments.

To evaluate the accuracy of the GPS-R measurements, we compare the derived sea-surface wave frequencies with the buoy measurements and the WRF model data provided by the CWB of Taiwan (https://ocean.cwb.gov.tw/V2/data_interface/datasets#). The moored buoy is located at (22.075 °N, 121.583 °E) and provides in situ measurements of sea-surface wave heights, maximum and mean periods, and maximum and mean wind speeds at a time resolution of one hour. Moreover, the WRF model data include sea-surface wave height and period values at a time resolution of three hours and a spatial resolution of

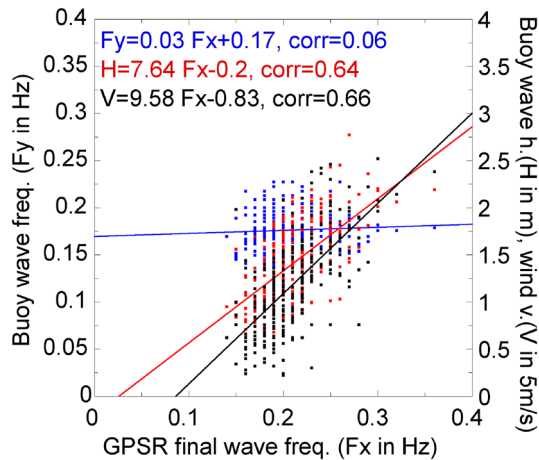


Fig. 11 Three scatter plots for the measured buoy wave frequencies (F_y , referring to the left y-axis), wave heights (H , referring to the right y-axis), and wind speeds (V , referring to the right y-axis) versus the averaged GPS-R sea-surface wave frequency values (F_x , referring to the x-axis) are shown in blue, red, and black, respectively. Three corresponding least-squares fitting lines, line equations, and the obtained correlative coefficients are also shown

0.25° in latitude and longitude. Therefore, there is only one position at (22.00°N , 121.50°E) for the WRF model data collocated with the GPS-R observations from the Lanyu-SW system.

Figure 11 illustrates three scatter plots and the corresponding least-squares fitting lines for the measured buoy wave frequencies, wave heights, and wind speeds versus the averaged GPS-R sea-surface wave frequency values. The GPS-R observations coincide with the in situ buoy measurements to within half hour in time and 2 km in space in the collocation range. The results show that the buoy wave height and wind speed measurements have high linear correlation coefficients of 0.64 and 0.66, respectively, in the GPS-R sea-surface wave frequency measurements. The correlation results are better than or close to the earlier investigations by Clarizia et al. (2014), who obtained correlation coefficients of 0.44, 0.36, and 0.65 between U.S. National Data Buoy Center (NDBC) buoy measurements and wind speed estimates using space GNSS-R DDM average, DDM variance, and training edge slope of integrated time-delay waveform, respectively. Furthermore, the measured wave heights and wind speeds from buoys are approximately linear to the final GPS-R sea-surface wave frequencies and have ratios of 7.64 and 47.9, respectively. However, the buoy wave frequency measurements have a low linear correlation coefficient of 0.06 with the GPS-R wave frequency measurements, even though the mean final sea-surface wave frequency from the GPS-R measurements is 0.21 Hz and close to that (0.18 Hz) of the buoy measurements. Notably, the sea-surface wave frequency, wave height, and wind velocity measurements

from the CWB buoy are independent in situ measurements from the wave observation sensor, GPS positioning receiver, and wind sensor, respectively. The strong correlations of the measured buoy wave heights and wind speeds with the derived GPS-R sea-surface wave frequencies can prove the reliability of GPS-R measurements. As shown in Fig. 11, the distribution of the measured buoy wave frequencies is narrower than that of the derived GPS-R wave frequencies. Thus, the buoy wave observation sensor has different characteristics and acts as a filter.

Another evaluation of the GPS-R sea-surface wave frequency measurements using the WRF model data is shown in Fig. 12. Two scatter plots and the corresponding least-squares fitting lines for the modeled WRF wave frequencies and wave heights versus the averaged GPS-R sea-surface wave frequency values. The GPS-R observations coincide with the WRF model data within one and half hours in time and 4 km in the space in the collocation range. Notably, there are fewer WRF model data than the in situ buoy measurements in this experiment because of the longer temporal resolution of three hours. Thus, we used a wider collocation range of 4 km from the WRF validation position to increase the coincident GPS-R measurements. The correlation analysis results show that the modeled WRF wave heights have a linear correlation coefficient of 0.47 with the GPS-R wave frequency measurements. It is reasonable to have a lower correlation than that (0.64) of the buoy wave height correlation analysis because of the larger time and space collocation criteria. Notably, the mean wave frequency from the WRF model data is approximately 0.18 Hz and is almost the same as that from the buoy measurements, and the modeled WRF

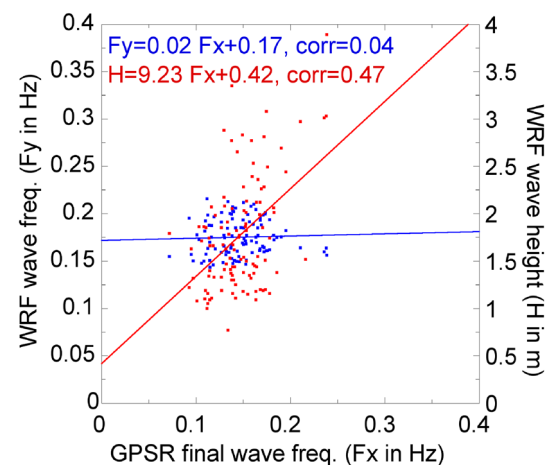


Fig. 12 Two scatter plots for the modeled WRF wave frequencies (F_y , left y-axis) and wave heights (H , right y-axis) versus the averaged GPS-R sea-surface wave frequency values (F_x , x-axis) are shown in blue and red, respectively. Two corresponding least-squares fitting lines, line equations, and the obtained correlative coefficients are also shown

wave frequencies also have a low linear correlation coefficient of 0.04 with the GPS-R wave frequency measurements. This result should be because the WRF model data produced by the CWB of Taiwan accept buoy measurements as inputs. Furthermore, as shown in Fig. 12, the mean final sea-surface wave frequency from the GPS-R measurements is 0.15 Hz and lower than that (0.21 Hz) in Fig. 11. This result could be because the collocated validation position of the WRF model data has a greater offshore distance and deeper ocean depth than those of the buoy location.

Summary and outlook

This study aims to exploit a software-based GPS-R receiving system and a new technique to measure the wave parameters of random sea-surface wave features. There are more convenient ways to become involved with software processing of GPS signals than to build the entire system from the bottom up, and the developmental portion of this research platform has the following specific objectives of interest: (a) the construction of a small, low-cost, transportable, and flexible GPS receiving system; (b) the development of L1-band C/A code signal acquisition and spectral analysis algorithms for GPS-R observations; (c) the estimates of sea-surface wave frequency, period, speed, and corresponding mapping products with wave propagation footprints of FFZ sizes. Future research should be performed to take advantage of GPS signal phase measurements and better assess the accuracy and precision of sea-surface state parameters. These implementations could lay more foundations, as we plan to build upon and add more functionality and refinement in the future. Additionally, we see involvement in software-based receivers as a long-term investment, as this tool kit opens up for a variety of new applications and advanced research topics within GPS- and other GNSS-related studies.

Acknowledgements The work was supported in part by MOST 107-2111-M-008-030 and 106-2923-M-008-001-MY3 from the Ministry of Science and Technology, Taiwan, R.O.C., and in part by a grant from the Asian Office of Aerospace Research and Development of the U.S. Air Force Office of Scientific Research (AOARD/ARFL FA2386-18-1-0115). The authors also acknowledge the German Research Foundation (DFG) for funding project DEAREST (SCHU 1103/15-1). The authors would also like to express their indebtedness to the CWB, Taiwan, for providing the data and supporting space and utility to operate the GPS-R systems.

Data availability The 4.096-MHz I-Q data obtained on DOY 346, 2019, from the Lanyu-ENE and Lanyu-SW systems can be downloaded from <http://isl.csrnr.ncu.edu.tw/en-us/data.html>.

References

- Borre K, Akos D, Bertelsen N, Rinder P, Jensen SH (2007) A software-defined GPS and Galileo receiver: a single-frequency approach. ISBN 978-0-8176-4390-4. Birkhauser
- Clarizia PC, Ruf CS, Jales P, Gommenginger C (2014) Spaceborne GNSS-R minimum variance wind speed estimator. *IEEE Trans Geosci Remote Sens* 52(11):6829–6843. <https://doi.org/10.1109/TGRS.2014.2303831>
- Goda Y (1990) Random waves and spectra, in *Handbook of Coastal and Ocean engineering, Volume 1: Wave Phenomena and Coastal Structures*. Edited by Herbich JB, 175–212, ISBN 0-872-01461-4. Gult Publishing Company, Houston
- Hristov HD (2000) *Fresnel zones in wireless links, zone plate lenses and antennas*. ISBN 0-89006-849-6. Artech House, Inc., Norwood
- Lin B, Katzberg SJ, Garrison JL, Wielicki BA (1999) Relationship between GPS signals reflected from sea surfaces and surface winds: Modeling results and comparisons with aircraft measurements. *J Geophys Res* 104(C9):20713–20727
- Longuet-Higgins MS (1957) The statistical analysis of a random, moving surface. *Phil Trans Roy Soc London, Ser A* 966:321–387. <https://doi.org/10.1098/rsta.1957.0002>
- Martín-Neira M (1993) A passive reflectometry and interferometry system (PARIS): application to ocean altimetry. *ESA Journal* 17:331–355
- Mei CC (1990) Basic gravity wave theory, in *Handbook of Coastal and Ocean Engineering, Volume 1: Wave Phenomena and Coastal Structures*. Edited by Herbich JB, 1–62, ISBN 0-872-01461-4. Gult Publishing Company, Houston
- Press WH, Teukolsky SA, Vetterling WT, Flannery BP (1992) *Numerical Recipes in C: The Art of Scientific Computing*, 2nd edn, ISBN 0-521-43108-5. Cambridge Univ Press, New York
- Rice SO (1944) Mathematical analysis of random noise. *Bell Syst Tech J* 23:282–332. <https://doi.org/10.1002/j.1538-7305.1944.tb00874.x>
- Rius A, Aparicio JM, Cardellach E, Martín-Neira M, Chapron B (2002) Sea surface state measured using GPS reflected signals. *Geophys Res Lett* 29(23):2122. <https://doi.org/10.1029/2002GL015524>
- Trizna TB (1997) A model for Brewster angle damping and multipath effects on the microwave radar sea echo at low grazing angles. *IEEE Trans Geosci Remote Sens* 35(5):1232–1244. <https://doi.org/10.1109/36.628790>
- Tsui JBY (2000) *Fundamentals of Global Positioning System Receivers: A Software Approach*. ISBN 0-471-20054-9. John Wiley & Sons, Inc., New York
- Wickert J et al (2016) GEROS-ISS: GNSS Reflectometry, Radio Occultation, and Scatterometry onboard the International Space Station. *IEEE J Sel Topics Appl Earth Obs Remote Sens* 9(10):4552–4581. <https://doi.org/10.1109/JSTARS.2016.2614428>
- Zavorotny VU, Voronovich AG (2000) Scattering of GPS signals from the ocean with wind remote sensing application. *IEEE Trans Geosci Remote Sens* 35(3):951–964. <https://doi.org/10.1109/36.841977>

Publisher's Note Springer Nature remains neutral with regard to jurisdictional claims in published maps and institutional affiliations.



Lung-Chih Tsai is a professor at the National Central University, Taiwan. His research focuses on the study of the ionosphere and upper atmosphere: theory and instrument of ionospheric sounders, data processing and analysis to GPS receiver and radio occultation system, satellite beacon receiver, and JASON.



Harald Schuh is the Director of Department 1 “Geodesy” at GFZ German Research Centre for Geosciences in Potsdam, Germany, and professor for “Satellite Geodesy” at the University of Technology Berlin. He has been involved with geodetic space research for more than 35 years with a special focus on tropospheric and ionospheric modeling, VLBI (Very Long Baseline Interferometry), GNSS, and earth rotation.



Shin-Yi Su is currently an adjunct professor at National Central University after his retirement in 2010. He was the Principal Investigator of IPEI instrument onboard ROCSAT-1, measuring ionospheric ion density, velocity, temperature, and composition at 600 km altitude from 1999 to 2004. He has been using IPEI data to study the ionospheric irregularity properties extensively since then.



Jens Wickert is the head of GNSS remote sensing research and research director for “The Atmosphere in Global Change” of the GFZ German Research Center for Geosciences. In addition, he holds a professorship for “GNSS Remote Sensing, Navigation and Positioning” at the University of Technology Berlin. He is the Principle Investigator of several GNSS related research projects, including GPS Radio Occultation missions.



Hwa Chien is an associate professor at the National Central University, Taiwan. He currently serves as the director of the Advanced Research Center for Earth Sciences at NCU. His research focuses on the process-based air-sea interaction, techniques R&D of in-situ and remote sensing of oceanic environment and hydrodynamics in coastal zone and estuary.



M. Mahdi Alizadeh received his Ph.D. in Geodesy from Vienna University of Technology in 2013. He spent about three years as a post-doc fellow at the University of Technology in Berlin. He is currently an assistant professor at KNToosi University of Technology.



Chao-Han Liu is an Academician at Academia Sinica and K.T. Li Chair Professor at National Central University in Taiwan. His fields of interest are radio science and solar-terrestrial physics.